Special Section: Contaminants in the Vadose Zone

Yuxin Wu*
Susan Hubbard
Dawn Wellman

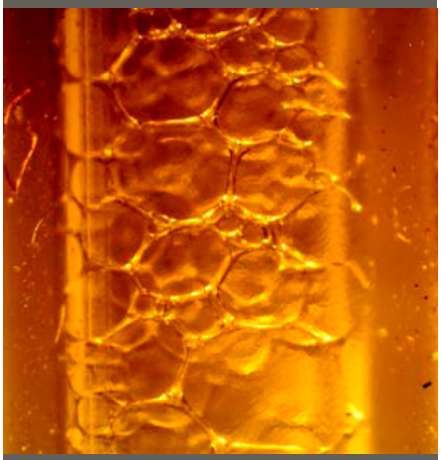

Geophysical monitoring of foam injection and transformation was studied in column experiments. Our results demonstrated the sensitivity of electrical and time-domain reflectometry signals to foam injection and transformation in porous media and suggest the potential of these methods for monitoring the response of the subsurface to foam-based remediation treatments.

Y. Wu and S. Hubbard, Earth Sciences Division, Lawrence Berkeley National Lab., 1 Cyclotron Rd., Berkeley, CA 94720; D. Wellman, Environmental Systems Group, Pacific Northwest National Lab., PO Box 999, Richland, WA 99352. *Corresponding author (ywu3@lbl.gov).

Vadose Zone J.
doi:10.2136/vzj2011.0160
Received 15 Nov. 2011.

© Soil Science Society of America
5585 Guilford Rd., Madison, WI 53711 USA.
All rights reserved. No part of this periodical may be reproduced or transmitted in any form or by any means, electronic or mechanical, including photocopying, recording, or any information storage and retrieval system, without permission in writing from the publisher.

Geophysical Monitoring of Foam Used to Deliver Remediation Treatments within the Vadose Zone

Foam is a promising vehicle for delivering amendments into the vadose zone for in situ remediation; it is an approach being considered for in situ treatment and stabilization of metals and radionuclides located within the deep vadose zone of the Department of Energy's Hanford Site in the state of Washington. A central aspect of evaluating the effectiveness of this approach is the ability to monitor foam distribution, its transformation, and the reactions that it induces in the subsurface, ideally in a noninvasive manner. In this study, we performed laboratory experiments to evaluate the potential of geophysical methods (complex resistivity and time-domain reflectometry [TDR]) as tools for monitoring foam-assisted amendment delivery in the deep vadose zone. Our results indicated great sensitivity of electrical methods to foam transportation and evolution in unsaturated porous media that were related to foam bubble coalescence and drainage processes. Specifically, we observed (i) a decrease in electrical resistivity (increase in electrical conductivity) by more than an order of magnitude in both silica sand and natural sediment matrices during foam transportation; (ii) an increase in resistivity (decrease in conductivity) of more than twofold during foam coalescence and drainage; and (iii) a distinct phase and imaginary conductivity signature related to the evolution of water films on sediment grains during foam injection and evolution processes. To assist with the interpretation of these data, TDR measurements were used to monitor moisture content, which provided complementary information about foam distribution and drainage. Our results clearly demonstrated the sensitivity of electrical and TDR signals to foam transportation and evolution in unsaturated porous media and suggest the potential of these methods for monitoring the response of a system to foam-based remediation treatments at field scales.

Abbreviations: DOE, Department of Energy; EDL, electrical double layer; EM, electromagnetic; IP, induced polarization; TDR, time-domain reflectometry.

The vadose zone is a critical conduit for transport of pollutants from the ground surface to groundwater. Contaminants in the vadose zone are susceptible to mobilization through diffusion or during recharge and water table fluctuations, posing a long-term threat to groundwater. Effective remediation of vadose zone contaminants is one of the greatest challenges in environmental remediation (Looney and Falta, 2000; Zhong et al., 2010, and references therein). This challenge is exacerbated in deep vadose zone environments, where surface excavation and offsite treatment is economically unfeasible. In the deep vadose zone, conventional amendment delivery strategies, which rely on the injection of water-based solutions, are fraught with hydrologic and geochemical challenges. Preferential flow in the deep vadose zone is pervasive (Hendrickx and Flury, 2001), which often leads to preferential percolation of the injected treatment through permeable pathways that often bypass the most contaminated regions (Glass et al., 1988; Zhong et al., 2009b). Furthermore, the application of large volumes of fluid can potentially mobilize contaminants in the vadose zone, enhancing their transport to the underlying aquifers (Hanson et al., 1993; Qafoku et al., 2003, 2007).

There are several attractive characteristics of using foam to deliver remedial treatments to the vadose zone. Foam is defined as a two-phase system in which gas bubbles are separated by thin liquid films (Birkerman, 1973). It has a higher viscosity than the water or gas phase alone and has been used in the oil industry to enhance sweep efficiency during oil recovery (Smith, 1988; Hirasaki, 1989). Using foam as a delivery vehicle can enhance the infiltration efficiency of remedies by promoting sweeping efficiency in low-permeability zones (Yan et al., 2006). Also, the flow of foam can potentially be better controlled through manipulation of pressure gradients in the subsurface (Zhong et al., 2009a). Moreover, the use of foam as a delivery vehicle significantly reduces the volume of water required, thus

mitigating contaminant mobilization to the groundwater through water flushing.

Successful development of foam as a remedial treatment delivery vehicle requires an understanding of foam dynamic behavior in heterogeneous porous media. For example, can foam be delivered to a target contaminated location before the collapse of the foam bubbles? Can the foam bubble size be optimized for transportation in sediments having a known pore size distribution? When the bubbles collapse, might drainage be significant enough that it could mobilize contaminants downward? These and other questions are currently being addressed by research such as Zhong et al. (2010).

An additional consideration is associated with the ability to monitor and eventually predict the delivery, emplacement, and long-term performance of foam in situ, as needed to evaluate the treatment performance. Conventional techniques for subsurface remediation monitoring rely on wellbore-based approaches to collect samples or make measurements. Because of their limited spatial extent, these methods often provide only limited information for the understanding of key controls on subsurface flow and transport. This is especially true in the vadose zone, where vertical infiltration pathways can form as a result of variable saturation and heterogeneity and where fluid recovery during sampling can be challenging.

The application of geophysical methods to improve the characterization and monitoring of near-subsurface properties and remediation processes has gained much interest in recent years (Rubin and Hubbard, 2005). Because geophysical data can be collected from many platforms (such as at the ground surface, between wellbores, and within wellbores), these methods can interrogate the subsurface variables across a variety of spatial scales and resolutions. One of the main advantages of using geophysical monitoring over conventional measurements is its ability to provide spatially extensive information about the subsurface in a minimally invasive manner at a comparatively high resolution. A particularly attractive feature of geophysical methods for subsurface process monitoring is their ability to collect a suite of continuous data sets at the same location as a function of time, or "time-lapse" data sets that can illuminate changes in the system. Time-lapse geophysical approaches have been effectively used for hydrologic investigations to monitor vadose zone water infiltration at the Department of Energy (DOE) Hanford Site and elsewhere (Hubbard et al., 1997a, 1997b; Binley et al., 2002; Daniels et al., 2005; Kowalsky et al., 2005; Lambot et al., 2006; Rucker et al., 2011). Time-lapse geophysical methods have also been successfully used to monitor biogeochemical transformations associated with remediation treatments (Williams et al., 2005, 2009; Hubbard et al., 2008; Wu et al., 2010, 2011). Together, these studies have demonstrated the potential of geophysical methods—particularly time-lapse complex conductivity (or resistivity) and TDR methods—for improving our understanding of amendment distribution, induced biogeochemical reactions, and the underlying control of heterogeneity on subsurface environmental remediation processes.

In this study, we performed laboratory experiments to evaluate the applicability of geophysical methods as tools for monitoring foam transportation and evolution in vadose zone sediments. This is a prelude to field-scale geophysical monitoring of a foam-based remedial pilot study that is planned for a deep vadose zone contaminated site at Hanford (Zhong et al., 2010). We explored the sensitivity of both electrical and TDR signals to foam transportation and subsequent transformations and investigated whether the methods are suitable tools for monitoring foam-delivery-assisted subsurface remediation at the field scale.

Theoretical Background

For this study, we focused on exploring complex conductivity (or resistivity) and TDR methods based on their predicted sensitivities to major changes during foam injection and transformation, mostly moisture content and mineral–water–air interfacial properties. Complex conductivity (σ^*) measures the charge conduction behavior, and for a porous geological medium it is oftentimes frequency dependent. The measured $\sigma^*(\omega)$ can be represented as

$$\sigma^*(\omega) = \sigma'(\omega) + i\sigma''(\omega) \quad [1]$$

where ω is the angular frequency; σ' is the measured real part of $\sigma^*(\omega)$, being the conduction component; σ'' is the measured imaginary part of $\sigma^*(\omega)$, being the induced polarization (IP) component; and $i = \sqrt{(-1)}$.

The factors that contribute to the complex conductivity signatures vary depending on sample conditions. For saturated media, electrical charge transport is primarily determined by (i) the electrolytic conduction (σ_{el}) via the interconnected fluid-filled pore space (a purely real term), and (ii) a complex interfacial conduction (σ_{int}^*), occurring near the grain–electrolyte interfaces. The σ_{el} is dependent on the conductivity of the electrolyte (σ_w) saturating the porous media (Archie, 1942), whereas σ_{int}^* represents an interfacial charge conduction and polarization behavior within the electrical double layer (EDL) at the grain–electrolyte interface (Schwarz, 1962; Wong, 1979; Slater et al., 2005). For partially saturated vadose zone material with negligible metal content (which is the case we studied here), the dominant electric pathway is through water films on mineral surfaces. As such, the real (or charge conduction) component of the electrical signal is mainly determined by the number and thickness of these water film paths, their continuity and tortuosity, and the salinity of the fluid in the films.

Although only a few studies have explored the imaginary (or charge polarization) component of the electrical signal in unsaturated media, a positive correlation between induced polarization and water content has been documented (Parkhomenko, 1971; Titov et

al., 2004; Ulrich and Slater, 2004). Foam systems inherently provide a significant amount of gas bubbles and, therefore, air–water interfaces. Potential polarization at these interfaces should be considered because of the existence of negative surface charges at air–water interfaces based on zeta potential measurements (Manciu and Ruckenstein, 2006; Creux et al., 2007). Previous research has investigated the potential effect of the air–water interface on electrical resistivity (Knight, 1991) and has suggested that conduction at the air–water interface might be responsible for the resistivity hysteresis effects observed during drainage and imbibition. To the best of our knowledge, however, no study has investigated low-frequency charge polarization behavior at this interface.

Based on these previous findings, our conceptual model of the complex conductivity (or resistivity) response to foam injection in porous media is as follows. When foam is injected into a porous medium, in addition to the growth of the water films on sediment grains due to the moisture content increase, the newly introduced water films that exist between the foam bubbles serve as additional conduits for charge conduction, thereby causing an increase in electrical conductivity (or decrease in resistivity). As the foam coalesces and the bubbles grow in size with time, the number and thickness of these conduits within the pore space will decrease, thus leading to a decrease in conductivity (increase in resistivity). Foam injection and subsequent coalescence and drainage could alter charge polarization in two ways: (i) by changing the thickness and extensiveness of the water films on sediment grains; or (ii) by changing the volume of air–water interfaces that are charged, which could contribute to overall charge polarization.

Time-domain reflectometry, a commonly used electromagnetic (EM) method, measures the apparent dielectric permittivity of a medium based on the measured velocity of a guided EM wave. With this approach, an EM signal is sent to a waveguide and travels along the rods in transverse electromagnetic mode. With the length of the probe and travel time known, the EM wave velocity can be calculated, which can be used to estimate dielectric properties. A commonly used petrophysical model for estimating water content from dielectric constant values is the complex refractive index model (Birchak et al., 1974):

$$\sqrt{\kappa} = \theta\sqrt{\kappa_w} + (\phi - \theta)\sqrt{\kappa_a} + (1-\phi)\sqrt{\kappa_s} \qquad [2]$$

where θ is water content, ϕ is porosity and κ_w, κ_a, κ_s, and κ are the dielectric constants of water, air, sediments, and the bulk sample, respectively. Another well-used relationship between dielectric permittivity and water content is the empirical Topp's equations. The general Topp's equation (Topp et al., 1980) is given as

$$\kappa = 3.03 + 9.3\theta + 146\theta^2 - 76.7\theta^3 \qquad [3]$$

As foam is introduced into low moisture content porous media, we expect the moisture content to increase, thereby increasing the dielectric constant and decreasing the propagation velocity. Subsequent bubble transformations could cause additional changes in the moisture content if drainage occurs during bubble coalescence and growth.

Materials and Methods

Experimental Apparatus

Two apparatus were built for the experiments, one for TDR and the other for complex resistivity measurements (Fig. 1).

The TDR apparatus was made from polycarbonate and is a short and wide column with dimensions of 6.4 cm (height) by 11.5

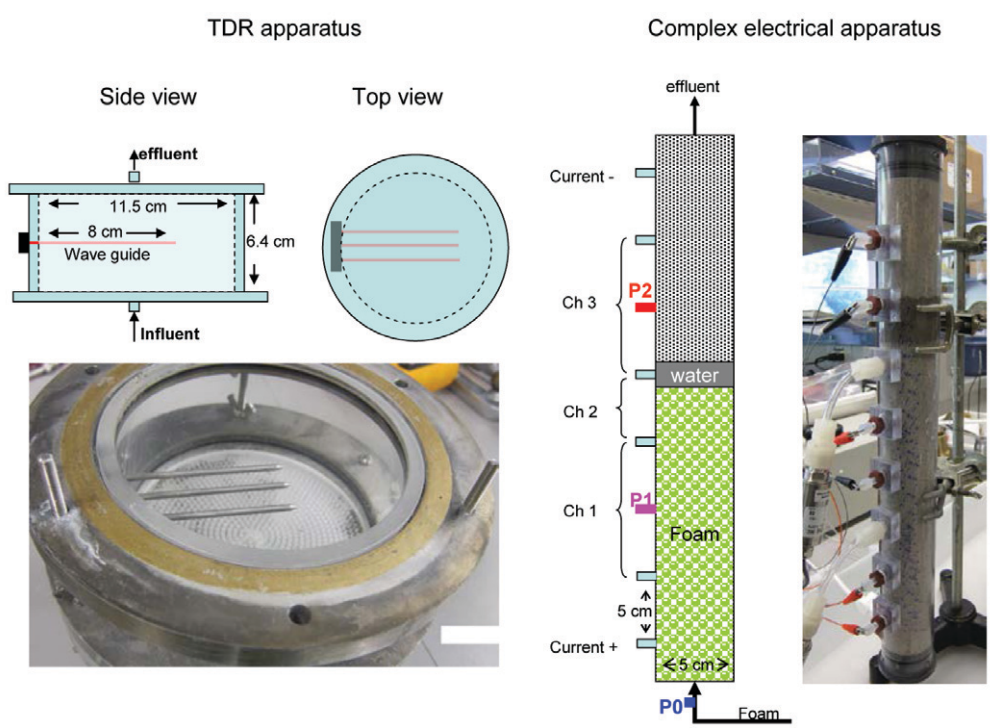

Fig. 1. Apparatus design for time-domain reflectometry (TDR) (left) and complex resistivity (right) measurements; P0, P1, and P2 are the locations of the pressure transducers used for pressure monitoring. The drawing of the electrical column indicates a single time point, where foam is traveling from the bottom to the top of a sand-packed column and where a water front has formed at the advancing front of the foam plume.

cm (i.d.) An 8-cm buriable waveguide with three stainless steel rods was installed in the middle of the column for guiding radar wave propagation during TDR measurements. Polycarbonate filter plates (with ~1-mm pore size) were installed at both ends of the column to help confine the sediments as well as distribute the injected foam evenly across the column before it enters the sediments. The column for complex resistivity measurements had a dimension of 44 cm (height) by 5 cm (i.d.). Eight ports with an interval of 5 cm were installed along the side wall of the column for electrical measurements and pressure monitoring. Electrical signals were measured at three different channels (1, 2, and 3 from bottom to top; Fig. 1), and the pressure was monitored at three different locations using pressure transducers (P0, P1, and P2; Fig. 1).

Solid Matrix

To investigate the effects of different moisture retention capacities on foam behavior and geophysical signals, both silica sand and Hanford Site sediments were used for the experiments. Ottawa sand was first used in both columns followed by Hanford Site sediments. Ottawa sand with a fairly uniform grain size at ~600 μm was acquired from U.S. Silica, and the average porosity of the Ottawa sand packed column was ~38%. Site sediments used in the experiments were acquired from boreholes close to the DOE Hanford Site BC cribs area. The sediments used in this research were the same K2 sediments used by Zhong et al. (2010), which are primarily sand with silt and clay. These sediments had an average porosity of 29.6%, with a mean grain size and standard deviation of 1180 and 150 μm, respectively. The Hanford sediments had larger average grain size, lower porosity, and poorer sorting relative to the Ottawa sand. Because the Ottawa sand surface was relatively smooth and had fewer fines and micropores than the Hanford sediments, low moisture retention capacity was expected for the silica sand samples.

Surfactant and Foam Generation

The foaming agent was a water-based solution of a surfactant mix including cocamidopropyl betaine, coconut diethanolamide, and sodium lauryl sulfate (Stepan Company). This solution was blended in a modified blender (L'equip 306500 RPM) with continuous supply of N_2 as the gas component of the foam. The size of the produced foam bubble is dependent on the blending rate; an 800 rpm blending rate was used to produce an ~200-μm average bubble size for this study. The size of the foam bubble was confirmed with an optical microscope. The fresh foam produced from this setup was primarily ball shaped, with a volumetric water content of ~10 to 15%, or equivalently, a foam quality of 90 to 85%. The produced foam was then introduced into the measurement apparatus driven by gas pressure or by using a peristaltic pump.

Optical Imaging of Foam Evolution

Imaging using an optical microscope (Motic DM143) was performed to help understand the foam evolution after injection. A silicon tubing (2-mm i.d.) was placed horizontally under the microscope, and freshly generated foam was injected into the tube and was observed and photographed with time to document the foam transformation after injection.

Experimental Procedure

For both TDR and electrical measurements, three scenarios were tested: foam only, foam in silica sand packed columns, and foam in site sediment packed columns. For the foam-only scenario, pure foam was injected into the empty columns and electrical and TDR measurements were collected regularly with time. The columns were subsequently cleaned, dried, and packed with Ottawa sand. During packing, the columns were tapped a few times after each ~1 cm of sand was introduced. The sand was very dry, with negligible moisture content (<0.5%). After packing, foam was introduced into the bases of both columns and injection continued until steady foam flow was observed for at least 10 min at the effluent ends. The TDR and complex resistivity measurements were collected continuously before, during, and after foam injection into the Ottawa sand columns. In the final experiment, the columns were cleaned and repacked with Hanford sediments using the same procedure described above. The sediments had an initial moisture content of ~3 to 4% based on gravimetric measurements. Foam was injected into the columns at ~12 mL/min using a peristaltic pump. For all three scenarios, foam was injected into the apparatus from the bottom, and injection was continued until stable foam was eluted from the top of the apparatus for at least 10 min.

Complex Resistivity and Time-Domain Reflectometry Measurement Approaches

Electrical measurements were collected with a National Instruments dynamic signal analyzer (DSA, NI 4461) at the three different channels (Channels 1, 2, and 3) using Ag–AgCl electrodes placed along the length of the electrical column (Fig. 1). A preamplifier was used to boost the input impedance to 10^9 Ω to avoid significant current leakage into the measurement circuitry. Water-column-based repeatability tests for this system indicated that errors were <0.3 mrad for the phase and 0.5% for conductivity when low frequency was used (<500 Hz). Each measurement was composed of a phase shift (ϕ) and a magnitude ($|\sigma|$) component. The measurements were recorded relative to a precision reference resistor for 30 frequencies spaced at equal logarithmic intervals from 1 to 1000 Hz. Spectral data below 1 Hz was not recorded because of the short duration of the foam transport process within the column (~30 min) and the long time required to acquire low-frequency (<1-Hz) data. Because the DSA board has only one channel available for sample measurements, a parallel port relay board was built as a multiplexer to switch between the three measurement channels along the length of the column as shown in Fig. 1. The data acquisition rate was about 1 data set per minute; therefore each data cycle for all three channels required ~3 min to collect. The real and imaginary components of the complex conductivity represent the magnitude of the conduction and the polarization of the sample, respectively, and were determined from

$$\sigma' = |\sigma| \cos\phi \quad [4]$$

$$\sigma'' = |\sigma| \sin\phi \quad [5]$$

and

$$\phi = \arctan\left(\frac{\sigma''}{\sigma'}\right) \sim \frac{\sigma''}{\sigma'} \quad (\text{when } \phi \text{ is small}) \quad [6]$$

The TDR data were collected with a Trase system (Soilmoisture Equipment Corp.) using an 8-cm, three-prong buriable TDR waveguide probe. The TDR was connected to a multiplexer and programmed to record waveforms every minute. Inflections in the recorded waveform were automatically picked and converted to dielectric constant values. These values were then used with the petrophysical relationship given in Topp's equation (Eq. [3]) to estimate moisture content. Ideally, relationships between moisture content and dielectric constant would be developed for each material under consideration (here, the Ottawa sand and Hanford samples). With our objective of assessing relative changes in moisture associated with foam injection, coalescence, and drainage, however, the use of an established petrophysical relationship such as Topp's equation was deemed acceptable.

Results and Discussion

Imaging of Foam Evolution

Foam can only be stable for a certain period of time; coalescence and breakage will eventually occur. Time-lapse optical microscopic observations of foam injected into a horizontal capillary tube illustrate this evolutionary process during a 15-min time frame. Figure 2 shows that the freshly injected foam bubbles were dominantly spherically shaped and had an average diameter of ~200 μm. With time, the bubbles coalesced and fluid drainage occurred, causing bubble size growth and a bubble shape change from sphere to polyhedron. Based on tests conducted in tubes of other diameters (5, 25.4, and 51 mm; images not shown), the maximum size of the foam bubble is constrained by the size of the pore in which the bubble resides.

Based on a conceptual model extracted from the optical microscopy study of foam in a capillary tube, Fig. 3 schematically shows the evolution of foam in a low-moisture-content pore space between grains. The conceptual model assumes that under very low moisture content, water exists as thin films on sediment grains, with the pore space filled with air (Fig. 3A). Once foam is injected, the pore spaces become filled with ball-shaped air bubbles separated by water films, and the water saturation of the sediment is greatly enhanced (Fig. 3B). Note that bubble breakage and regeneration can occur at pore throats. Therefore, the foam bubbles within the pore space are a mixture of those originally injected and those

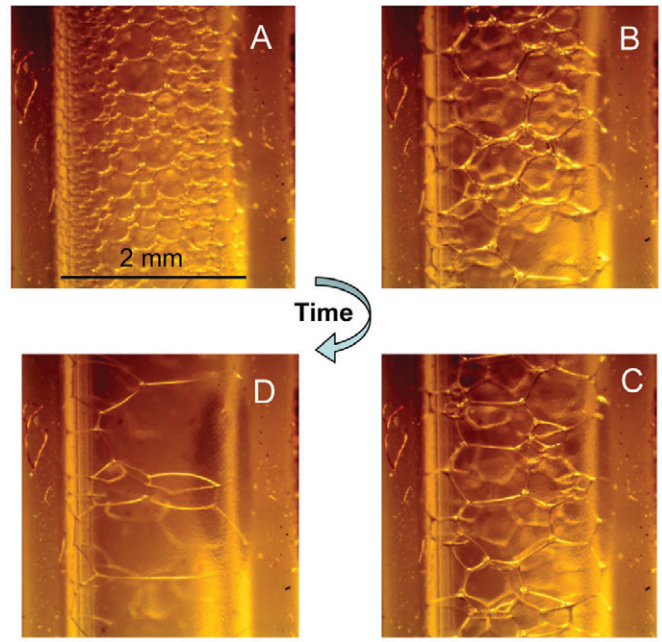

Fig. 2. Foam transformation with time after injection within a horizontal 2-mm stopped capillary tube: (A) freshly produced foam, and after approximately (B) 5 min, (C) 10 min, and (D) 15 min.

newly generated during transport through pore throats. Once foam injection ceases, ball foam bubbles coalesce and transform with time into larger polygons, and the excess water drains onto the adjacent sediment grains (Fig. 3C). With time, these polygons become larger (Fig. 3D) and will eventually break, with all the water absorbed by sediments or draining out.

Pure Foam Phase

Foam was produced using the protocol described above and injected into the empty TDR and electrical columns until the columns were filled with the foam. After the columns were completely filled, the injection continued for another ~10 min to reach a

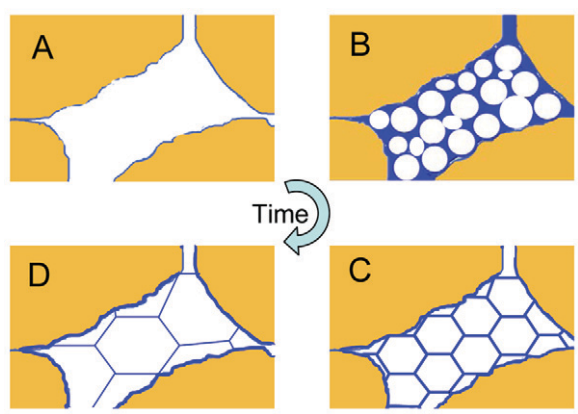

Fig. 3. Schematic of foam evolution in pore space: (A) baseline pore space filled with air, with a thin liquid film on sediment grains; (B) pore space filled with ball-shaped foam during injection phase; (C, D) foam transformation from sphere to larger and more polygonal-shaped bubbles.

stable state. Visually, the transformation in bubble shape and size was apparent with time once foam injection stopped. The original foam had an approximate average diameter of ~200 μm, and it grew to a few centimeters, constrained by the size of the columns, within about 20 min. The evolution of the foam in the two experimental columns was similar based on visual observations, although the bubbles grew to larger sizes in the TDR column relative to the electrical column due to the larger diameter of the TDR column. Large changes in both electrical and TDR signals were observed during this process (Fig. 4). The electrical resistivity increased by more than two orders of magnitude from ~100 to >10,000 Ω m (Fig. 4A). This change was interpreted to be due to the transformation of the fresh, ball-shaped foam bubbles into larger polygons and the concomitant drainage of excess water from the bubble films. This transformation also significantly reduced the number of water films between gas bubbles (i.e., available electric conduits) in the measurement channels, leading to a large resistivity increase. The phase response at 1 Hz from the column is also shown in Fig. 4A. No observable phase response was recorded for the initial stage of the experiment, which indicates that the relatively large bubble size (~200 μm and larger) provided only limited surface area, which was not significant enough to produce a detectable IP signal. The phase values observed during the later stage of the experiment were probably due to EM coupling because of the large contact resistance between electrodes and the foam during this stage (Fig. 4A).

Both the electrical resistivity and moisture responses are consistent with our conceptual model. Moisture content calculated based on TDR measurements revealed a reasonable initial value at ~10%; however, this value dropped to just above zero fairly quickly (Fig. 4B), indicating limited resolution of the TDR measurements at low moisture content, which is partially due to the short length (8 cm) of the TDR probes. Compared with the TDR measurements, the electrical resistivity provided continuous measurements of resistivity changes during foam transformation even at very low moisture content. Estimation of the moisture content based on electrical resistivity can be made on the establishment of petrophysical correlations between electrical resistivity and moisture content in the context of specific foam characteristics.

Foam in Silica Sand Columns

The experimental results from the sand columns are shown in Fig. 5 and 6 (electrical data) and Fig. 7 (TDR data).

Due to the dryness of the silica sand used in the experiments, the contact resistance between measurement electrodes and the sand was quite high. This caused large noise levels in measurements, therefore large variations in the measured resistivity values of the column before foam arrival at the electrodes (Fig. 5). Nevertheless, large resistivity values at >10,000 Ω m were observed before the arrival of the foam at the measurement channels (Fig. 5). Foam arrival at the measurement channels significantly reduced the electrical resistivity to ~1000 Ω m or below, and sequential decreases

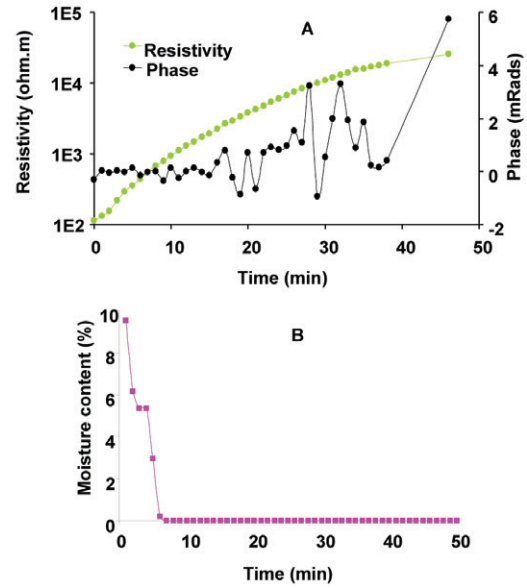

Fig. 4. Changes in (A) electrical resistivity and phase at 1 Hz (data from Channel 1 of the electrical column) and (B) moisture content obtained by time-domain reflectometry after foam injection into the columns.

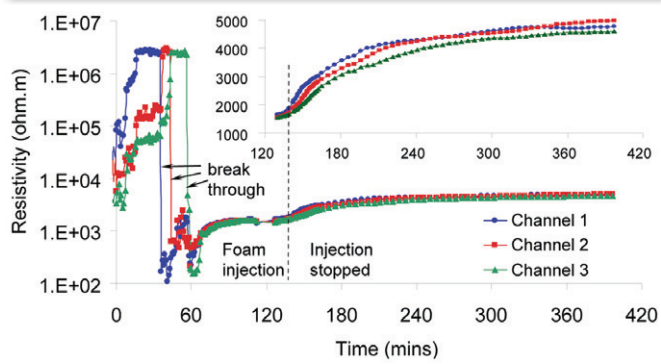

Fig. 5. Changes in electrical resistivity magnitude at 1 Hz on a logarithmic scale during foam injection and transportation in a silica sand packed column. Injection started at time $T = 0$ min. Imbedded figure shows changes in resistivity on a linear scale after foam injection was stopped at ~130 min.

in the resistivity were observed from Channels 1 to 3 (bottom to top) as the foam front migrated sequentially through the measurement channels. Note that between 30 and 60 min, there was a short period of resistivity rebound. This rebound was most evident for Channel 1, less significant for Channel 2, and barely noticeable for Channel 3. Although the exact reason warrants further investigation, it might be related to the unsteady breakthrough of the water front at the bottom channels because the water front was thin and uneven in the low part of the column.

After the initial foam breakthrough, the resistivity of all three channels started to increase slowly until foam injection stopped at ~130 min. The imbedded subfigure in Fig. 5 shows the changes in resistivity after foam injection ceased, and a resistivity increase from ~1500 to ~5000 Ω m was observed. Note that there was

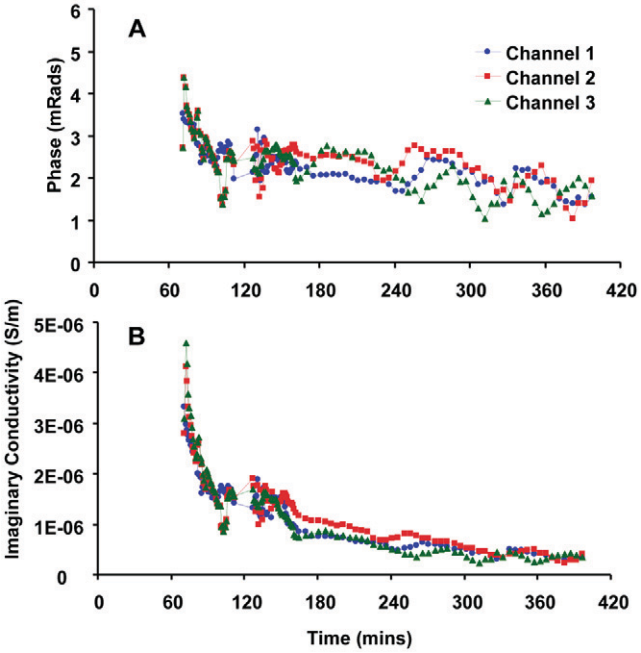

Fig. 6. Changes in (A) phase and (B) imaginary conductivity at 1 Hz during foam injection into sand-packed columns.

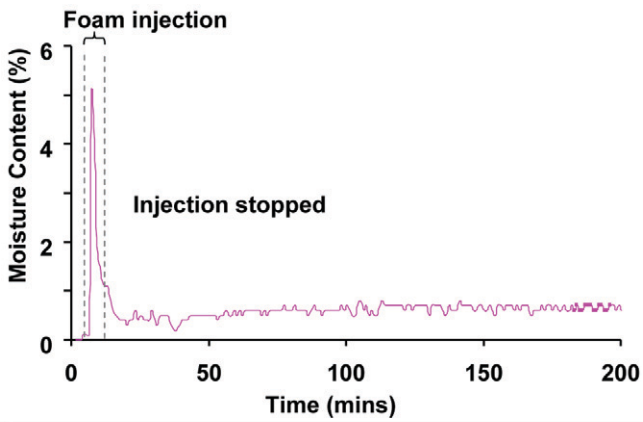

Fig. 7. Moisture content changes associated with foam injection into the silica sand packed time-domain reflectometry column.

a slight but sequential decrease in the resistivity from Channels 1 to 3 (Fig. 5) at any given time stamp during foam injection and during most of the post-injection stage. This could be related to the characteristics of the water front during its arrival at the three different channels. The water front forms ahead of the foam due to bubble breakage and liquid accumulation and has higher water content than the foam itself (Zhong et al., 2009b). As the foam traveled farther into the column and sequentially passed Channels 1 to 3, the water front became wider and contained more liquid. This resulted in a higher level of saturation of the sand in the upper part of the column (Channel 3) relative to the lower part (Channel 1) and therefore a sequential decrease in electrical resistivity from Channels 1 to 3 because resistivity is primarily controlled by the saturation level. In addition, the effects from the initial packing heterogeneity could contribute to the differences in resistivity as well. It is also interesting to note that the resistivity of all three channels increased steadily during continuous foam injection after the foam breakthrough in the column. This is also related to the water front because the water front has higher water content than the foam itself, therefore the initial water content of the sand acquired from the arrival of the water front was the highest, i.e., lowest resistivity, right after the breakthrough of the water front (Fig. 5). Subsequent arrival and passing of the lower-water-content foam carried some of the liquid away, thus reducing the water content of the sand, which was responsible for the increase in resistivity before foam injection stopped. Based on the findings from the experiments with pure foam (Fig. 4), the gradual increase in electrical resistivity after foam injection had stopped was related to the increase in foam bubble size from foam coalescence and water drainage, i.e., reduction of the moisture content as well as the number of available electrical pathways through the water films between gas bubbles.

In addition to large changes in resistivity, we also observed small IP effects due to foam injection into the silica sand matrix; this IP response was recorded after the foam front passed the current injection electrodes at the top (at ~65 min after injection; Fig. 6). A maximum phase response of ~4 mrad and imaginary conductivity at 4×10^{-6} S/m were observed during initial foam breakthrough (at ~65 min) and this value gradually dropped to ~1 mrad for phase and close to zero for imaginary conductivity during foam coalescence and drainage ($T > 130$ min). Reliable baseline phase and imaginary conductivity data cannot be measured before foam arrival at the current electrodes due to the large contact resistance between the electrodes and the dry sand. The observed polarization signal during foam injection was due to the formation of water film on the sand grains, thus establishing mineral–fluid interfaces and EDL structures, a prerequisite for charge polarization (Lyklema, 1995, p. 3.208). The EDL is established through surface protonation–deprotonation as well as ion exchange processes on mineral surfaces when they are in contact with water. The subsequent decrease in phase can be related to the reduced availability of interconnected water films during foam coalescence and drainage.

Figure 7 shows changes in moisture content in the TDR column packed with silica sand during foam injection and subsequent transformation. The initial moisture content was close to zero due to the dryness of the sand. During foam injection, a maximal moisture content of ~5% was observed, which dropped to a sustained level at ~0.5% after the foam injection ceased (Fig. 7). The 5% moisture content peak was probably associated with the water front, similar to the observation from the electrical column. Interestingly, only a short peak at 5% moisture content was observed, which indicates the thinness of the water front. This is reasonable because the TDR column was short in height and there was only ~3 cm between the inlet and the TDR probes; therefore, only a thin water front was developed before the arrival of the water front at the probes. Also, compared with the electrical column (where the electrical signals

were measured across a "distance" between the two potential electrodes, which provided a longer resident time of the water front in the measurement area), the TDR probe measured at a single location along the column. As such, the thin water front is interpreted to have passed by the probes fairly quickly, leading to a short peak of high moisture content.

Experimental data from silica sand packed columns demonstrated the sensitivities of both the complex resistivity and the TDR measurements to foam injection and subsequent transformations. The foam appears to have transported through the column steadily, as evidenced from sequential and significant decreases in resistivity from Channels 1 to 3. The water front had a higher moisture content than foam itself and caused the initial large decrease in the resistivity when it arrived at the measurement channels. This water front was also captured by the TDR measurements as a sharp rise in water content. After the breakthrough of the water front at the electrical and TDR sensors, a resistivity increase and moisture decrease was observed during the subsequent arrival and breakthrough of the foam itself (Fig. 5 and 7). The moisture level of the TDR column dropped to a low level at (~0.5%) after foam injection had stopped (Fig. 7). This was attributed to the low moisture retention capacity of the silica sand and thus the drainage of the excess water accumulated during foam coalescence. The low TDR-obtained final moisture estimates compared relatively well with gravimetrically measured values (~0.6% assuming a density of 1 g/mL for the surfactant mix), suggesting that the application of Topp's relation (Eq. [4]) was reasonable for our study.

These observations are consistent with our conceptual model: foam injected into a porous medium causes the growth of water films on sand grains, and the newly introduced water films between gas bubbles serve as additional conduits for charge conduction. Both changes significantly decreased the electrical resistivity (Fig. 5), increased the moisture content (Fig. 7), and led to a phase response by saturating the sand grains with thin water films (Fig. 6). During subsequent foam coalescence and bubble size growth, the number and thickness of these water films and charge conduits within the pore space decreased, resulting in an increase in resistivity and decrease in the phase and TDR-estimated moisture content (Fig. 5, 6, and 7).

Foam in Hanford Site Sediments

In the last experiment with the Hanford sediments, pressure data at three different locations (the inlet and one-third and two-thirds of the column; Fig. 1) were collected for the electrical column and are shown in Fig. 8. The inlet pressure increased continuously to ~276 kPa as the foam was transported farther into the column during injection. The pressure at one-third and two-thirds of the distance from the bottom of the column increased to ~221 and 110 kPa, respectively. Figure 8 also shows the pressure responses associated with the different phases of the experiment. Pressure started to increase on the arrival of the foam at the individual

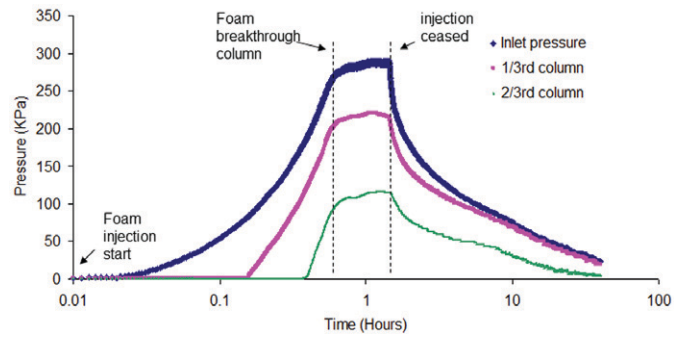

Fig. 8. Pressure at three different locations during foam injection into the Hanford sediment packed column.

pressure sensors and increased consistently for all three locations until the foam breakthrough at the top of the column at ~34 min after injection started (Fig. 8). A slight increase in pressure was observed at all three locations during continuous injection after foam breakthrough at the top of the column. This slight increase in pressure was potentially related to the increase in moisture content of the sediment due to water adsorption during this period, which may enhance the pressure requirement for foam transportation. Because the effluent port was kept open, the pressures started to decrease slowly at all three locations after injection stopped, indicating bubble coalescence and slow gas release from the effluent end of the column.

Electrical data at 1 Hz collected during this experiment are shown in Fig. 9 and moisture content calculated from the TDR column run in parallel with the electrical column is shown in Fig. 10. Our discussion focuses on the electrical column, for which the experiment can be divided into three different phases (Fig. 9): (i) an injection phase from 0 to ~0.5 h while foam was injected upward from the bottom of the column, with eventual breakthrough at the top of the column; (ii) a stable foam injection phase from 0.5 to 1.5 h, and (iii) a post-injection–coalescence phase after 1.5 h.

Distinctive electrical signals were observed during the three different phases of foam injection. During the initial injection phase, the resistivity decreased from >1000 to <100 Ω m sequentially across Channels 1 to 3 (Fig. 9A) and real electrical conductivity increased by an order of magnitude from 0.001 to ~0.01 S/m (Fig. 9C). In addition to changes in resistivity and conductivity, there was a slight phase increase from ~5.5 to 7 mrad during foam injection and a large increase in imaginary conductivity by more than an order of magnitude from $\sim 4 \times 10^{-6}$ to $\sim 7 \times 10^{-5}$ S/m. After breakthrough of the foam at the top of the column, a continuous but much slower decrease in resistivity (increase in real conductivity) was observed during extended foam injection. Slight increases in phase and imaginary conductivity were also observed during this period. It is interesting to note that the resistivity behavior during the continuous foam injection phase was different in the site-sediment-packed column relative to the

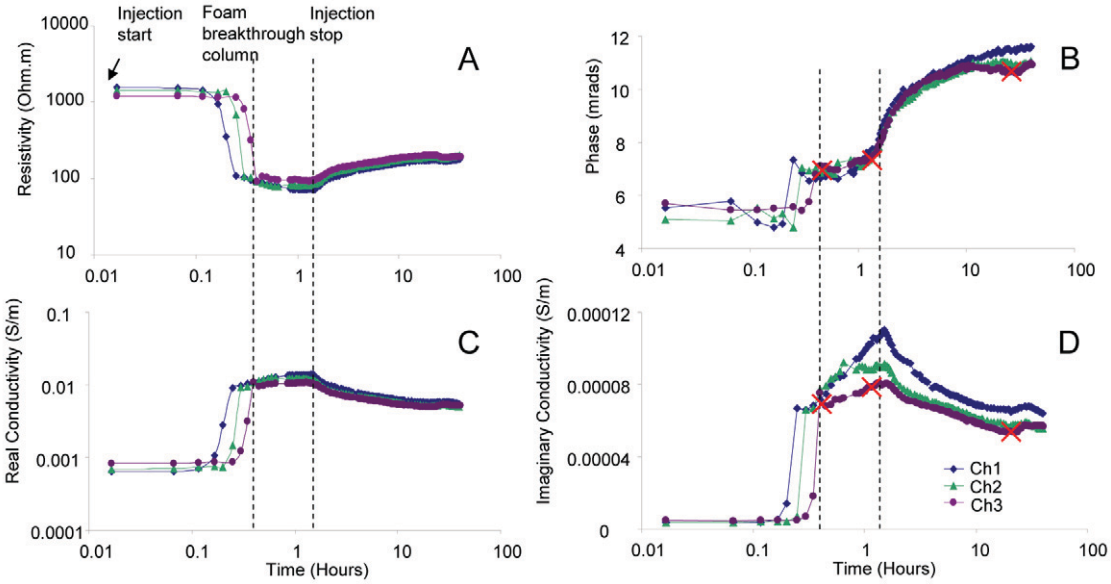

Fig. 9. Electrical measurements at 1 Hz during foam injection into a sediment-packed column: (A) resistivity magnitude; (B) phase; (C) real conductivity, and (D) imaginary conductivity. Note that resistivity and real conductivity are plotted on a logarithmic scale. The red × symbols mark 0.45, 1.1, and 17.6 h from the initiation of foam injection.

sand-packed column: the resistivity continued to decrease in the site sediment column while it started to increase in the sand column. This could be related to the different moisture retention capabilities between the site sediment and Ottawa sand. Due to a high moisture retention capacity, the site sediment continued to absorb liquid and increased in moisture content during foam injection until a stable moisture level was achieved, leading to a continuous resistivity decrease before foam injection was stopped. During continuous foam injection after the arrival of the water front in the Ottawa sand, however, the sand started to lose some of its moisture, previously acquired from the water front, due to its low moisture retention capacity, leading to a resistivity increase during this process. After the foam injection ceased, slow but continuous rebounds of resistivity and real conductivity were observed in the site sediment column similar to the observation from the sand column. Phase continued to increase but imaginary conductivity started to decrease during this post-injection period.

The TDR measurements indicated that the baseline moisture content of the sediment was ~3.2% before foam injection, which quickly increased to ~10% during foam injection and then reached a sustained value of ~9% for the rest of the experiment. Gravimetric water content analysis of samples recovered from the electrical column showed a moisture content of ~10%, similar to the TDR-based estimates.

The different measurements lead to an integrated interpretation of foam behavior in porous material. During the injection phase, the large decrease in resistivity, more than one order of magnitude, was attributed to the growth of water films on sediment grains as well as the addition of new water films (i.e., electrical conduits) between

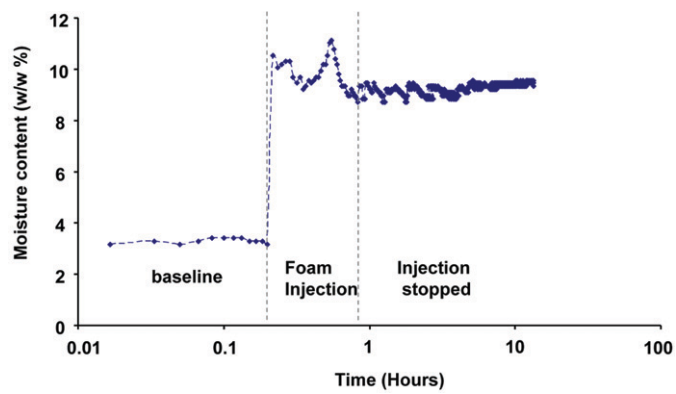

Fig. 10. Moisture content change during foam injection into a sediment-packed column as calculated from time-domain reflectometry measurements.

gas bubbles within the pore space, as illustrated in Fig. 3B. The large increase in imaginary conductivity is indicative of increased extensiveness and interconnectivity of water films on sediment grains due to the moisture content increase during foam injection, thus increasing the wetted surface area and its connectivity available for charge conduction and polarization. A small electrical phase increase was observed during this period as well. Electrical phase magnitude is roughly the ratio between the imaginary and real conductivities (Eq. [6]), both of which increased simultaneously during foam injection. Because the rate of increase for the imaginary conductivity was slightly higher than that of the real conductivity, a small increase in the phase response was observed.

During stable foam injection after its breakthrough at the top of the column, the resistivity continued to decrease slowly and the real conductivity, phase, and imaginary conductivity continued to

increase. During this stage, the bulk pore spaces were filled with foam bubbles and can be considered relatively stable. The major change during this stage was the continuous hydration of the sediments and the increase in the magnitude of the water films and probably their thickness and interconnectivity. Imaginary conductivity (Fig. 9D) is exclusively related to the conduction and polarization along these water films and its continuous increase can be considered evidence of water film growth during this stage. As mentioned above, the continuous hydration of the soil particles was interpreted to be responsible for the slight decrease in resistivity (increase in conductivity) during this period.

We also attributed the slight increase in phase to hydration effects. After foam injection ceased, all electrical parameters reverted toward initial conditions except the phase response, which continued to increase. Changes in electrical signatures during this stage were related to the coalescence of the foam bubbles. As discussed above for the silica sand column and shown in Fig. 3C and 3D, the number and thickness of water films (i.e., electrical conduits) between gas bubbles decreased during foam coalescence and resulted in an increase in resistivity and decrease in conductivity. Note that the resistivity never recovered to the baseline value because the water released from bubble coalescence was absorbed by adjacent soil particles, maintaining the moisture content at a higher level and thus enhanced electrical conductivity relative to the baseline. The coalescence and breakage of the foam bubbles could disrupt the connectivity between sediment grains previously enhanced by the water films between foam bubbles. This could reduce the interconnectivity of the water films on sediment grains, therefore reducing the amount of interconnected surface available for charge polarization and thus the magnitude of surface conduction and polarization, i.e., the imaginary conductivity, along these water films.

During this stage the real conductivity decreased faster than the imaginary conductivity, causing an increase in the phase response, the ratio between the two. The sustained moisture within the column during this stage was confirmed by the TDR measurements (Fig. 10). Note that the TDR response for the sediment-packed column was dramatically different from that of the sand-packed column (Fig. 5). While the moisture content of the sand column decreased significantly due to low moisture retention capacity during bubble coalescence and drainage, the moisture level was sustained in the sediment-packed column. This is an indication that the site sediment has a much higher moisture retention capacity relative to the Ottawa sand and that water released from foam coalescence and breakage was absorbed by adjacent sediment grains, thus maintaining a higher moisture content in the longer term.

Discussion of the complex resistivity data has focused on those collected at 1 Hz because this is the frequency at the typical range used for field-scale IP surveys, and thus interpretation of the experimental results at this frequency is indicative of the expected responses from field-scale applications. Spectral responses from 1 to 1000 Hz were collected during the experiments, however, and examples of spectral phase and imaginary conductivity data from Channel 3 at selected times (0.45, 1.1, and 17.6 h, Fig. 9) are shown in Fig. 11.

The spectral responses shown in Fig. 11 are representative of all three channels during the experiments. Both the phase and imaginary conductivity spectra showed a certain level of frequency dependency, with increased values at higher frequencies. Measurement noise at high frequencies, typically >100 Hz, from electromagnetic coupling could be high, however; therefore interpretation of the high-frequency data should be exercised with caution. Nevertheless, both phase and imaginary conductivity seem to be weakly frequency dependent and no characteristic critical frequency, i.e., predominant relaxation time length, exists. This type of spectral response has been observed previously for saturated and unsaturated unconsolidated samples (Vanhala, 1995; Slater and Lesmes, 2002; Ulrich and Slater, 2004) and was attributed to superposition of multiple relaxations across various time length scales (Lesmes and Morgan, 2001). Note that at the low frequency range from 1 to 100 Hz, relative changes between different times were consistent across different frequencies. Therefore, the above analysis of electrical data at 1 Hz is representative of the spectral responses.

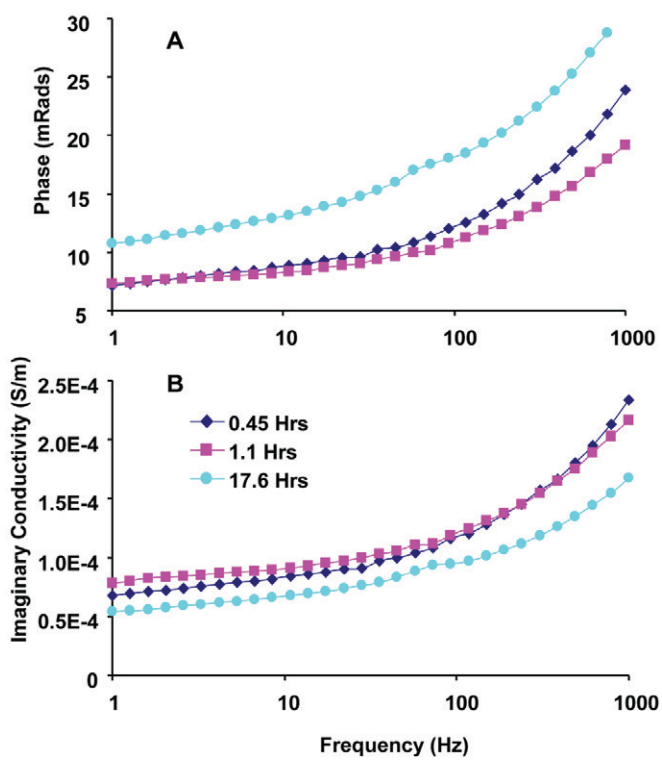

Fig. 11. Spectral data for (A) phase and (B) imaginary conductivity from Channel 3 at 0.45, 1.1, and 17.6 h from the initiation of foam injection into a sediment-packed column.

Summary and Conclusions

A series of column experiments were conducted to measure the complex resistivity and TDR signatures during foam injection and evolution to evaluate the potential of these methods for monitoring foam-assisted amendment delivery for vadose zone remediation at field scales. Foam was produced by blending a surfactant mix under N_2 atmosphere and was injected into two columns for electrical and TDR monitoring. Three different scenarios were tested: pure foam injection, foam injected into a silica sand column, and foam injected into a site-sediment-packed column. Complex resistivity and TDR measurements were performed for all these cases and were compared and related to the foam transportation and evolution processes.

From our experimental results, the following conclusions about the utility of the electrical and TDR methods for monitoring foam distribution and evolution can be made:

- The initial injection of foam into unsaturated porous media (both silica sand and Hanford sediments) resulted in a large decrease in resistivity (increase in electrical conductivity) due to the moisture content increase of the soil particles as well as the addition of newly created water films between gas bubbles within the pore spaces, which act as additional electrical conduits. Continuous foam injection after the initial breakthrough resulted in additional changes in the electrical signals due to continued hydration of the soil particles until a stable state was reached.

- After foam injection ceased, the resistivity increased due to the reduced number and thickness of the water films between gas bubbles during foam coalescence and drainage. The resistivity during bubble coalescence and breakage was still much lower than the baseline values of the original sediment due to enhanced moisture content of the sediments. The electrical resistivity response to foam injection and subsequent transformation was similar for both samples tested, suggesting its suitability for monitoring foam behavior in porous media with different moisture retention capacities.

- A distinct phase and imaginary conductivity signature was observed for natural sediment grains during foam injection and transformation. These responses were indicative of the dynamics of the water films on sediment grains and between gas bubbles within the pore spaces. The different magnitude and behavior of the polarization between the Ottawa sand and the Hanford sediment highlights the important role of sediment characteristics (texture, initial saturation, particle size distribution, etc.) on polarization signals.

- The TDR measurements were useful for estimating moisture content changes associated with foam injection and subsequent drainage. The TDR data were useful for providing estimates of moisture content but were not sensitive to subtle changes due to local redistribution of moisture and water films within the pore structures.

It is worth noting that different geophysical attributes (resistivity, phase, and dielectric constant) revealed different sensitivities to the various stages of foam injection. For example, while the resistivity change during foam injection was significant and can be used to track the foam injection process, the concurrent phase change was small and could not be used for tracking foam injection. Phase responses have demonstrated the potential for tracking critical biogeochemical transformations in other studies, however, and are expected to be useful for monitoring long-term geochemical transformations after foam injection has stopped. Our study suggests that the joint use of multiple monitoring methods, in this case complex resistivity and TDR, should greatly reduce interpretation uncertainty and improve process understanding associated with foam remediation.

Through our study, we have demonstrated the sensitivity of both electrical and TDR methods to foam injection and evolution in unsaturated porous media and the utility of these methods to monitor foam-assisted remedy delivery for vadose zone remediation. Foam-based remediation monitoring using geophysical methods is more complex than the study investigated here, however, for two reasons. First, the remediation treatments will lead to more complex (bio)geochemical reactions that can alter the pore and interfacial properties and, concomitantly, the geophysical response. For example, we expect the time-lapse phase response to be potentially useful for studying longer term biogeochemical transformations occurring on sediment grains due to foam injection. Second, the ratio of the geophysical measurement support scale to the characteristic scale of the foam distribution or remediation process is much larger at the field scale relative to the laboratory scales investigated here. This increased ratio will decrease the ability of the geophysical method to resolve sharp gradients or localized phenomena. Nevertheless, with the growing interest in using foam as a strategy to deliver remedial treatments into contaminated vadose zone environments, our study suggests that geophysical methods hold a significant potential for monitoring foam-based remediation technologies and suggests that further research is warranted.

Acknowledgments

This research was supported by the U.S. Department of Energy, Office of Environmental Management, EM-30 Technology Innovation and Development Office, and Richland Operations Office. Help from Elsa Cordova and Danielle Jansik at PNNL on site sediments and foam generation method is highly appreciated. We thank the associate editor Andrew Ramsburg. We also thank Dale Rucker and two anonymous reviewers for constructive comments.

References

Archie, G.E. 1942. The electrical resistivity log as an aid in determining some reservoir characteristics. Trans. Am. Inst. Min. Metall. Pet. Eng. 146:54–62.

Binley, A., G. Cassiani, R. Middleton, and P. Winship. 2002. Vadose zone flow model parameterisation using cross-borehole radar and resistivity imaging. J. Hydrol. 267:147–159. doi:10.1016/S0022-1694(02)00146-4

Birchak, J.R., C.G. Gardner, J.E. Hipp, and J.M. Victor. 1974. High dielectric constant microwave probes for sensing soil moisture. Proc. IEEE 62:93–98. doi:10.1109/PROC.1974.9388

Birkerman, J.J. 1973. Foams. Springer-Verlag, Berlin.

Creux, P., J. Lachaise, A. Graciaa, and J.K. Beattie. 2007. Specific cation effects at the hydroxide-charged air/water interface. J. Phys. Chem. C 111:3753–3755. doi:10.1021/jp070060s

Daniels, J.J., B. Allred, A. Binley, D Labrecque, and D. Alumbaugh. 2005. Hydrogeophysical case studies in the vadose zone. In: Y. Rubin and S.

Hubbard, editors, Hydrogeophysics. Springer, Dordrecht, the Netherlands. p. 413–440.

Glass, R.J., T.S. Steenhuis, and J.-Y. Parlange. 1988. Wetting front instability as a rapid and far-reaching hydrologic process in the vadose zone. J. Contam. Hydrol. 3:207–226. doi:10.1016/0169-7722(88)90032-0

Hanson, A., B. Dwyer, Z. Samani, and D. York. 1993. Remediation of chromium-containing soils by heap leaching: Column study. J. Environ. Eng. 119:825–841. doi:10.1061/(ASCE)0733-9372(1993)119:5(825)

Hendrickx, J.M.H., and M. Flury. 2001. Uniform and preferential flow mechanisms in the vadose zone. In: Conceptual models of flow and transport in the fractured vadose zone. Natl. Acad. Press, Washington, DC. p. 149–188.

Hirasaki, G.J. 1989. The steam-foam process. J. Pet. Technol. 41:449–456.

Hubbard, S.S., J.E. Peterson, E.L. Majer, P.T. Zawislanski, J. Roberts, K.H. Williams, and F. Wobber. 1997a. Estimation of permeable pathways and water content using tomographic radar data. Leading Edge 16:1623–1628. doi:10.1190/1.1437539

Hubbard, S.S., Y. Rubin, and E. Majer. 1997b. Ground-penetrating-radar-assisted saturation and permeability estimation in bimodal systems. Water Resour. Res. 33:971–990. doi:10.1029/96WR03979

Hubbard, S.S., K.H. Williams, M.E. Conrad, B. Faybishenko, J. Peterson, J. Chen, et al. 2008. Geophysical monitoring of hydrological and biogeochemical transformations associated with Cr(VI) bioremediation. Environ. Sci. Technol. 42:3757–3765. doi:10.1021/es071702s

Knight, R. 1991. Hysteresis in the electrical resistivity of partially saturated sandstones. Geophysics 56:2139–2147.

Kowalsky, M.B., S. Finsterle, J. Peterson, S. Hubbard, Y. Rubin, E. Majer, et al. 2005. Estimation of field-scale soil hydraulic and dielectric parameters through joint inversion of GPR and hydrological data. Water Resour. Res. 41:W11425. doi:10.1029/2005WR004237

Lambot, S., E.C. Slob, M. Vanclooster, and H. Vereecken. 2006. Closed loop GPR data inversion for soil hydraulic and electric property determination. Geophys. Res. Lett. 33:L21405. doi:10.1029/2006GL027906

Lesmes, D.P., and F.D. Morgan. 2001. Dielectric spectroscopy of sedimentary rocks. J. Geophys. Res. 106:13329–13346. doi:10.1029/2000JB900402</jrn

Looney, B.B., and R.W. Falta. 2000. Vadose zone science and technology solutions. Battelle Press, Columbus, OH.

Lyklema, J. 1995. Fundamentals of interface and colloid science. Vol. II. Solid–fluid interfaces. Academic Press, San Diego.

Manciu, M., and E. Ruckenstein. 2006. Ions at the air/water interface. J. Colloid Interface Sci. 304:541–544. doi:10.1016/j.jcis.2006.09.034

Parkhomenko, E.I. 1971. Electrification phenomena in rocks. Plenum Press, New York.

Qafoku, N.P., C.C. Ainsworth, and S.M. Heald. 2007. Cr(VI) fate in mineralogically altered sediments by hyperalkaline waste fluids. Soil Sci. 172:598–613. doi:10.1097/SS.0b013e31806db5b2

Qafoku, N.P., C.C. Ainsworth, J.E. Szescody, and O.S. Qafoku. 2003. Effect of coupled dissolution and redox reactions on $Cr(VI)_{aq}$ attenuation during transport in the Hanford sediments under hyperalkaline conditions. Environ. Sci. Technol. 37:3640–3646. doi:10.1021/es020935a

Rubin, Y., and S. Hubbard. 2005. Hydrogeophysics. Springer, Dordrecht, the Netherlands.

Rucker, D.F., J.B. Fink, and M.H. Loke. 2011. Environmental monitoring of leaks using time lapsed long electrode electrical resistivity. J. Appl. Geophys. 74:242–254. doi:10.1016/j.jappgeo.2011.06.005

Schwarz, G. 1962. A theory of the low-frequency dielectric dispersion of colloidal particles in electrolyte solution. J. Phys. Chem. 66:2636–2642. doi:10.1021/j100818a067

Slater, L.D., J. Choi, and Y. Wu. 2005. Electrical properties of iron-sand columns: Implications for induced polarization investigation and performance monitoring of iron-wall barriers. Geophysics 70:G87–G94.

Slater, L., and D.P. Lesmes. 2002. Electrical-hydraulic relationships observed for unconsolidated sediments. Water Resour. Res. 38(10):1213. doi:10.1029/2001WR001075

Smith, D.H. 1988. Surfactant-based mobility control: Progress in miscible-flood enhanced oil recovery. Am. Chem. Soc., Washington, DC.

Titov, K., A. Kemna, A. Tarasov, and H. Vereecken. 2004. Induced polarization of unsaturated sands determined through time domain measurements. Vadose Zone J. 3:1160–1168. doi:10.2136/vzj2004.1160

Topp, G.C., J.L. Davis, and A.P. Annan. 1980. Electromagnetic determination of soil water content: Measurement in coaxial transmission lines. Water Resour. Res. 16:574–582. doi:10.1029/WR016i003p00574

Ulrich, C., and L. Slater. 2004. Induced polarization measurements on unsaturated, unconsolidated sands. Geophysics 69:762–771.

Vanhala, H. 1995. Laboratory technique for measurement of spectral induced polarization response of soil samples. Geophys. Prospect. 43:655–676. doi:10.1111/j.1365-2478.1995.tb00273.x

Williams, K.H., A. Kemna, M.J. Wilkins, J. Druhan, E. Arntzen, A.L. N'Guessan, et al. 2009. Geophysical monitoring of coupled microbial and geochemical processes during stimulated subsurface bioremediation. Environ. Sci. Technol. 43:6717–6723. doi:10.1021/es900855j</jrn

Williams, K.H., D. Ntarlagiannis, L.D. Slater, A. Dohnalkova, S.S. Hubbard, and J.F. Banfield. 2005. Geophysical imaging of stimulated microbial biomineralization. Environ. Sci. Technol. 39:7592–7600. doi:10.1021/es0504035

Wong, J. 1979. An electrochemical model of the induced-polarization phenomenon in disseminated sulfide ores. Geophysics 44:1245–1265.

Wu, Y., J.B. Ajo-Franklin, N. Spycher, S.S. Hubbard, G. Zhang, K.H. Williams, et al. 2011. Geophysical monitoring and reactive transport modeling of ureolytically-driven calcium carbonate precipitation. Geochem. Trans. 12(7). doi:10.1186/1467-4866-12-7

Wu, Y., S.S. Hubbard, K.H. Williams, and J. Ajo-Franklin. 2010. On the complex conductivity signatures of calcite precipitation. J. Geophys. Res. 115:G00G04. doi:10.1029/2009JG001129

Yan, W., C.A. Miller, and G.J. Hirasaki. 2006. Foam sweep in fractures for enhanced oil recovery. Colloids Surf. A 282–283:348–359. doi:10.1016/j.colsurfa.2006.02.067

Zhong, L., M. Ankeny, A.T. Hart, L. Hull, J.E. Szecsody, M. Oostrom, et al. 2009a. Research plan: Foam delivery of amendments to the deep vadose zone for metals and radionuclides remediation. PNNL-18143. Pac. Northw. Natl. Lab., Richland, WA.

Zhong, L., N.P. Qafoku, J.E. Szecsody, P.E. Dresel, and Z.F. Zhang. 2009b. Foam delivery of calcium polysulfide to the vadose zone for chromium(VI) immobilization: A laboratory evaluation. Vadose Zone J. 8:976–985. doi:10.2136/vzj2008.0124

Zhong, L., J.E. Szecsody, F. Zhang, and S.V. Mattigod. 2010. Foam delivery of amendments for vadose zone remediation: Propagation performance in unsaturated sediments. Vadose Zone J. 9:757–767. doi:10.2136/vzj2010.0007